Hindawi
Journal of Sensors
Volume 2021, Article ID 8871166, 11 pages
https://doi.org/10.1155/2021/8871166

Research Article

A Gas Sensor for Application as a Propane Leak Detector

José Trinidad Guillen Bonilla,[1] **Héctor Guillen Bonilla**,[2] **Verónica-M. Rodríguez-Betancourtt**,[3] **Alex Guillen Bonilla**,[4] **Antonio Casillas Zamora**,[2] **Oscar Blanco Alonso**,[5] **and Jorge Alberto Ramírez Ortega**[2]

[1]*Departamento de Electrónica, CUCEI, Universidad de Guadalajara, 44410 Guadalajara, JAL, Mexico*
[2]*Departamento de Ingeniería de Proyectos, CUCEI, Universidad de Guadalajara, 44410 Guadalajara, JAL, Mexico*
[3]*Departamento de Química, CUCEI, Universidad de Guadalajara, 44410 Guadalajara, JAL, Mexico*
[4]*Departamento de Ciencias Computacionales e Ingenierías, CUValles, Universidad de Guadalajara, Carretera Guadalajara-Ameca Km 45.5, 46600 Ameca, JAL, Mexico*
[5]*Departamento de Física, CUCEI, Universidad de Guadalajara, 44410 Guadalajara, JAL, Mexico*

Correspondence should be addressed to José Trinidad Guillen Bonilla; jtgbonilla@gmail.com

Received 18 September 2020; Revised 17 January 2021; Accepted 21 January 2021; Published 13 February 2021

Academic Editor: Sang Sub Kim

A propane gas detector was built based on the semiconductor nickel antimonate oxide ($NiSb_2O_6$) by means of an analog electronic circuit. The gas detector was designed for monitoring atmospheres where the leakage of propane gas could possibly occur. The prototype's construction methodology is presented in 5 stages: (1) synthesis of $NiSb_2O_6$ oxide powders, (2) characterization of the powders by XRD and TEM, (3) manufacture and electrical characterization of the chemical gas sensor, (4) design of the analog circuit based on the electrical response of the gas sensor, and (5) functionality tests. The gas detector was built at low cost and showed excellent functionality. The operating conditions were as follows: 200°C, gas concentration of 5 ppm, electronic circuit gain of 5, and sensor sensitivity of 0.41.

1. Introduction

Health assurance systems are very important in industrial processes because they help prevent and eliminate emergencies, saving human lives and avoiding high economic costs. Among others, there are several types of health risks' scenarios: vibrations [1], short circuits [2], and fuel [3] and toxic gas leaks (propane, methane, ethane, carbon monoxide, and carbon dioxide) [4]. Exemplarily, propane gas detection systems play a very important role in the work with boilers because they prevent possible explosions due to failures in flame control [5]. These protection systems basically consist of a chemical sensor for propane gas and an electronic circuit for signal adaptation. The chemical sensor can be built based on semiconductor materials while the electronic circuit can be analog or digital.

Nowadays, semiconductor materials are being thoroughly studied to be applied as gas sensors. This is because materials like the semiconductor oxides show interesting chemical and physical properties when the surface of these materials come into contact with an oxidizing or reducing gas. In fact, their response is affected when the surface reacts chemically or physically with the molecules of test gases, varying the conductance and resistance as a function of concentration [6–8]. This change in electrical properties depends on the type of semiconductor material (*p*-type or *n*-type) [6, 7]. It has been reported in the literature that when a *p*-type semiconductor comes into contact with gas molecules like CO, the conductance diminishes and the electrical resistance increases [9]. Further, if the same semiconductor absorbs a gas such as O_2, then the conductivity rises and the electrical resistance decreases [6]. On the other hand, if an *n*-type semiconductor is subjected to CO_2 or O_2 atmospheres, the opposite of the *p*-type semiconductor will occur [10]. These behaviors are due to the nature of the charge carrier that the semiconductor possesses. According to the literature, several semiconductor materials have been proposed

for sensing applications, being some of them binary semiconductors (like NiO, CuO, WO_3, and TiO_2) [11], perovskites ($BaTiO_3$, $NdCoO_3$, and $ZnSnO_3$) [12–14], spinels ($AlCo_2O_4$, $NiFe_2O_4$, and $MgFe_2O_4$) [15–17], and trirutiles (MX_2O_6 where M can be Ni, Co, or Cu and X is replaced by Sb or Ta [18, 19], like $NiSb_2O_6$ [20], $CoTa_2O_6$ [21], and $NiTa_2O_6$ [22]). Regardless of the semiconductor material used for the sensor, an electronic circuit with desirable features is required for signal adaptation: low cost, high functionality, fast response, high sensitivity, excellent repeatability, high resolution, and easy construction.

In this work, a propane gas protection system, applicable for securing atmospheres free of such toxic gas, is proposed. The gas sensor was built on the basis of powders of synthesized nickel antimonate oxide ($NiSb_2O_6$), which is a trirutile-type semiconductor, and its signal adaptation was implemented using an analog circuit of operational amplifiers. The powders were characterized through X-ray diffraction (XRD) and transmission electron microscopy (TEM), while the sensor was physically characterized using static electrical tests. Based on the sensor's electrical response, an analog electronic circuit was chosen for adapting its signal. By combining the gas sensor and the electronic circuit, a prototype was designed for monitoring possible propane gas leaks. Its operating parameters were as follows: propane gas concentration of 5 ppm, temperature of 200°C, circuit gain of 5, and sensor sensitivity of 0.41. Experimental tests of the gas detector showed excellent functionality, repeatability, and fast response.

2. Materials and Methods

2.1. Materials. Figure 1 shows the electronic diagram of the propane gas detector which consisted of a sensor based on the nickel antimonate oxide ($NiSb_2O_6$) and an analog circuit. For the new device, it was required to have a 120/32 V transformer, a KBL610 diode bridge, an LM7812 regulator, an LM7912 regulator, four capacitors of $C_1 = C_2 = C_3 = C_4 = 2200\,\mu$F, two capacitors of $C_5 = C_6 = 0.1\,\mu$F, two resistors of $R_1 = R_2 = 516\,\Omega$, six resistors of $R_3 = R_4 = R_5 = R_6 = R_7 = R_8 = 1\,\text{k}\Omega$, a 1 kΩ trimpot calibrated to $R_{\text{Cal}} = 516\,\Omega$, and a 10 kΩ trimpot calibrated to $R_{\text{Gain}} = 500\,\Omega$.

2.2. Methodology. Figure 2 shows schematically the proposed methodology for the detector implementation. The methodology consisted basically of two stages: sensor fabrication and signal adaptation. In the sensor fabrication, the $NiSb_2O_6$ oxide powders were synthetized and characterized by XRD, the surface was analyzed through TEM, and pellets made with the powders were produced, whose electrical response was measured. In the signal adaptation, an analog circuit was built based on the sensor's electrical response, and it consisted of a Wheatstone bridge, an instrumentation amplifier, a comparator, and a DC supply source.

2.3. Chemical Sensor Fabrication. Figure 2 shows that the fabrication of the chemical sensor consisted of four phases: (1) synthesis of $NiSb_2O_6$ powders, (2) surface analysis, (3) pellet fabrication, and (4) electrical characterization. Each phase is described next:

(1) The $NiSb_2O_6$ powders were synthetized applying the microwave-assisted wet chemistry process described in references [23, 24]. The same concentrations, times, and equipment were used as indicated there

(2) The $NiSb_2O_6$ powders were characterized by XRD. In this case, Cu-α radiation with a wavelength of 1.5406 Å was used in a Panalytical Empyrean diffractometer. In addition, a 2θ sweep was performed in the range of 10 to 90°, with steps of 0.02° and a time of one second per step. The surface analysis was done using a transmission electron microscope (Joel Brand JEM-ARM200F) in a mode image. The nanoparticles' size was measured from the images acquired by the TEM. Previously, the individual nanoparticles of the $NiSb_2O_6$ powders were ultrasonically dispersed for 10 min and then deposited on a 300-mesh copper grid containing a formvar/carbon membrane (Ted Pella)

(3) To produce the pellets, 0.4 g of $NiSb_2O_6$ powders was compacted with a pressure of 20 tons during 170 min. Simple Ital Equip-25t equipment was used for that. The dimensions of the pellets were 12 mm in diameter and 0.5 mm in thickness. The pellets were placed on a metallic base inside the chamber. Two ohmic contacts made of high-purity colloidal silver paint (Alfa Aesar) were placed on the surface of the pellets, installing two electrodes on them so that there would be contact between the surface of the pellets and the test gas. The electrodes were separated in such a way that there was no contact between them, which allowed obtaining correct readings of the changes in electrical resistance of the sensor and, therefore, correct readings of sensitivity [24, 25]. The configuration of the sensing system is presented in Figure 3

(4) In order to measure the sensitivity of the chemical sensor, it was placed inside the propane detection system for the static tests, which were based on the variation of the resistance when the $NiSb_2O_6$ was exposed to propane flows at concentrations of 1, 5, 50, 100, 200, 300, 400, and 500 ppm and working temperatures of 100, 200, and 300°C. The sensitivity S was calculated using the following equation [24, 26]:

$$S = \frac{G_g - G_o}{G_o}, \tag{1}$$

where G_g and G_o are the material's electrical conductances (reciprocal of electrical resistance) in propane and air, respectively. Both terminals were connected to a Keithley 2001 digital multimeter and a voltage supply [23–25]. A measuring vacuum chamber with a vacuum capacity of 10^{-3} Torr was used. Gas concentration and partial pressure were controlled using a TM20 Leybold detector. The conductance was measured using a Keithley digital multimeter as a function of the operating temperature and the gas concentration (see Figure 3).

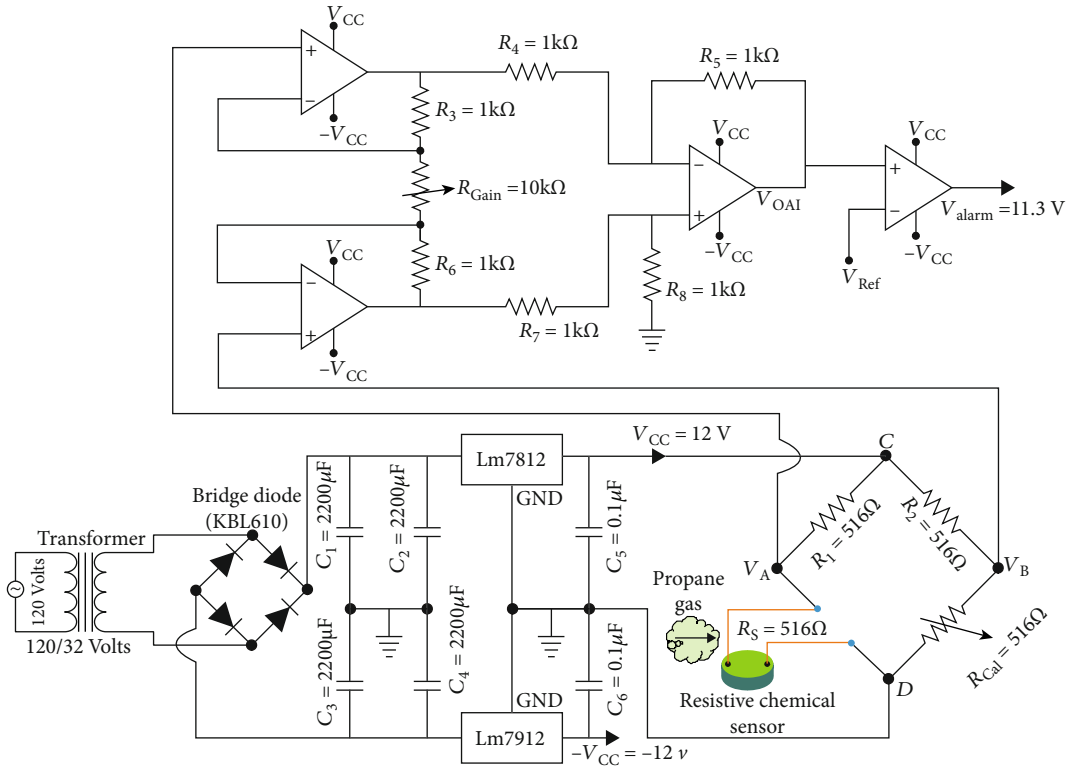

Figure 1: Propane gas detector.

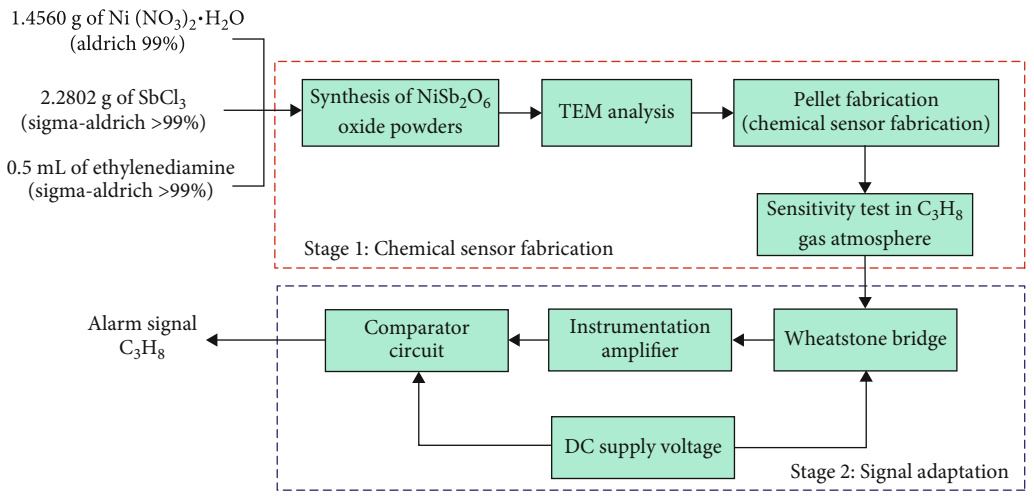

Figure 2: Stages required for the propane (C_3H_8) detection device.

2.4. Signal Adaptation. For the signal adaptation, an analog electronic circuit based on operational amplifiers was proposed. For its design, an operating temperature of 200°C, an operating concentration of 5 ppm, and a circuit's gain of 5 were considered. The sensor's resistance and sensitivity were $R_S = 516\,\Omega$ and $S \approx 0.41$, respectively. The electronic diagram is shown in Figure 1. Two stages were required for its application: calibration and detection.

2.4.1. Calibration. Firstly, the sensor was calibrated in an air atmosphere where the electronic detector did not produce the alarm signal, $V_{Alarm} = 0$. Then, the following steps were required: (a) the resistive chemical sensor was placed in atmospheres with no presence of propane gas, whose terminals were connected to a Wheatstone bridge; (b) the Wheatstone bridge was calibrated by varying R_{Cal} until the condition $V_{BA} = V_B - V_A = 0$ was met, calculating V_{BA} with

$$V_{BA} = V_B - V_A = V_{cc}\left(\frac{R_{Cal}}{R_2 + R_{Cal}} - \frac{R_S}{R_1 + R_S}\right) = 12\,\text{V}\left(\frac{516\,\Omega}{516\,\Omega + 516\,\Omega} - \frac{516\,\Omega}{516\,\Omega + 516\,\Omega}\right) = 0\,\text{V}, \quad (2)$$

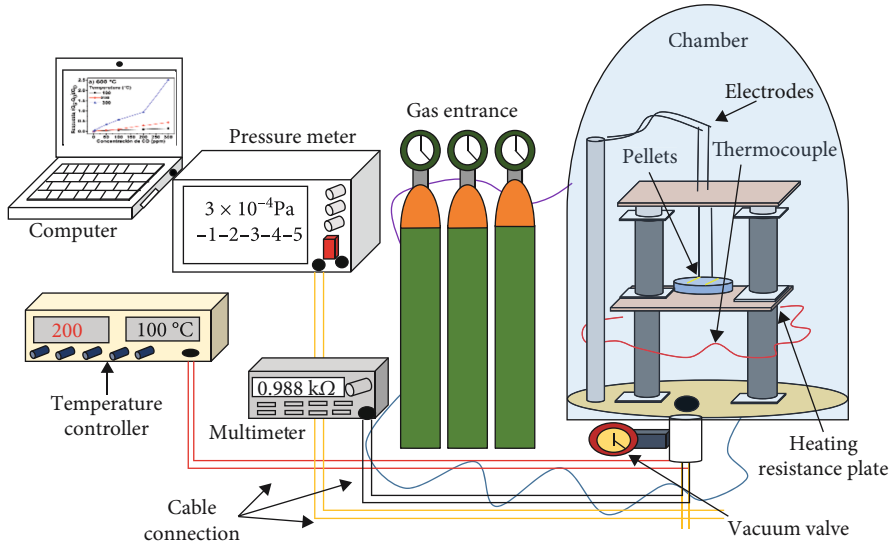

Figure 3: Schematic diagram of the sensing system for the static tests in propane atmospheres at controlled temperature and pressure.

where $V_{cc} = 12\,V$ is the supply voltage, R_1 and R_2 are precision resistors, R_S is the resistance of the chemical sensor, and R_{Cal} is a variable resistor for calibration; (c) an amplifier was used to compare voltages V_B and V_A, and it was also used to amplify the input voltage V_{OAI}, which was

$$\begin{aligned} V_{OAI} &= (V_B - V_A)\left(1 + \frac{2R_3}{R_{Gain}}\right) \\ &= 0\left(1 + \frac{2(1\,k\Omega)}{0.5k\Omega}\right) = 0(5) = 0\,V, \end{aligned} \tag{3}$$

where the term $(1 + (2R_3/R_{Gain})) = 5$ defines the gain, R_{Gain} is a variable resistance to increase the sensitivity of the propane detection device, R_3 is a precision resistor, and the condition $R_3 = R_4 = R_5 = R_6 = R_7 = R_8$ was true, and combining expressions (2) and (3), the voltage V_{OAI} was

$$\begin{aligned} V_{OAI} &= V_{cc}\left(\frac{R_{Cal}}{R_2 + R_{Cal}} - \frac{R_S}{R_1 + R_S}\right)\left(1 + \frac{2R_3}{R_{Gain}}\right) \\ &= 12\,V\left(\frac{516\,\Omega}{516\,\Omega + 516\,\Omega} - \frac{516\,\Omega}{516\,\Omega + 516\,\Omega}\right)\left(1 + \frac{2(1\,k\Omega)}{0.5\,k\Omega}\right) = 0\,V; \end{aligned} \tag{4}$$

(d) reference voltages V_{Ref} and V_{OAI} were compared using a comparator circuit such that the alarm signal V_{Alarm} was given by

$$V_{Alarm} = A_{ol}V_{OAI} = 10000(0\,V) = 0\,V, \tag{5}$$

where $A_{ol} \approx 10000$ is the operational amplifier's gain in an open loop. The detector device did not generate an alarm signal because the sensor was not detecting the propane gas.

2.4.2. Detection. In the detection stage, the resistive sensor based on the $NiSb_2O_6$ oxide was installed in atmospheres with the presence of C_3H_8 gas, installing the electronic device in a secure area. Then, the following steps were required: (a)

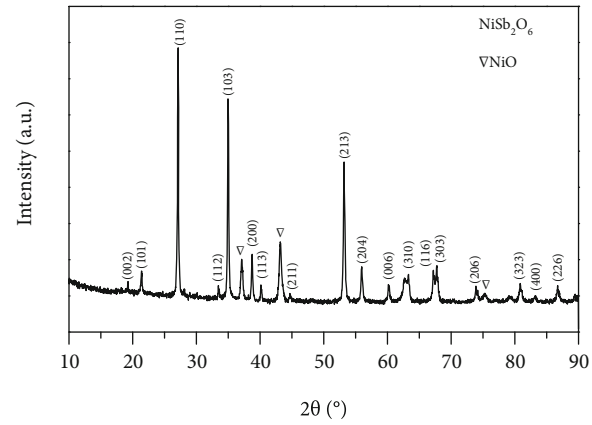

Figure 4: X-ray diffraction pattern of $NiSb_2O_6$ calcined at 800°C.

when the sensor detected the propane gas, the Wheatstone bridge had an imbalance by ΔR_S, satisfying the condition

$$\begin{aligned} V_{BA} &= V_B - V_A = V_{cc}\left(\frac{R_{Cal}}{R_2 + R_{Cal}} - \frac{R_S - \Delta R_S}{R_1 + R_S - \Delta R_S}\right) \\ &= 12\,V\left(\frac{1}{2} - \frac{516\,\Omega - \Delta R_S}{516\,\Omega + 516\,\Omega - \Delta R_S}\right) > 0\,V, \end{aligned} \tag{6}$$

such that $V_B > V_A$ is satisfied because $1/2 > (516\,\Omega - \Delta R_S)/(516\,\Omega + 516\,\Omega - \Delta R_S)$ is true; (b) the instrumentation amplifier produced an output voltage V_{OAI} given by

$$V_{OAI} = 60\left(\frac{1}{2} - \frac{516\,\Omega - \Delta R_S}{516\,\Omega + 516\,\Omega - \Delta R_S}\right) > 0, \tag{7}$$

where the value of 60 is obtained multiplying $V_{cc} = 12\,V$ and $(1 + (2R_3/R_{Gain}))$; (c) the alarm signal V_{Alarm} was produced by the comparator circuit shown in Figure 1, and based on equation (5), it is

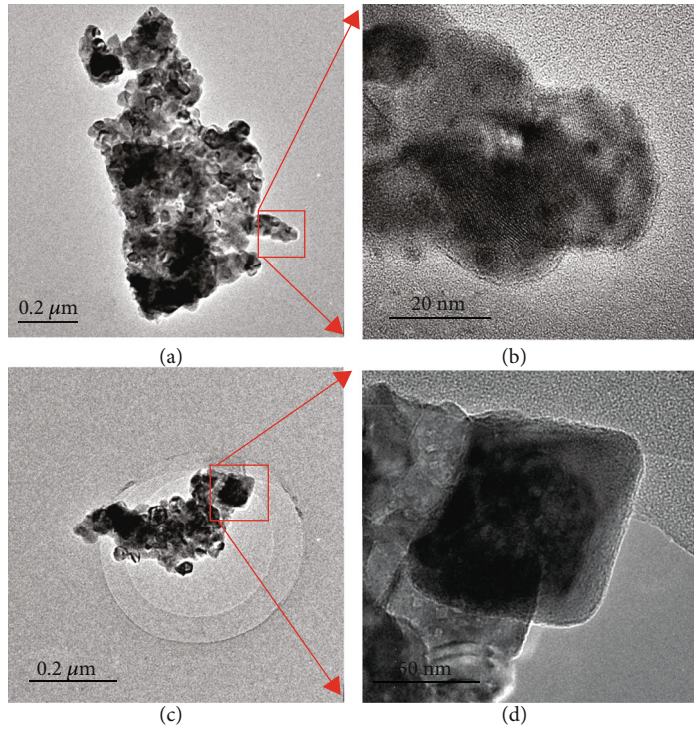

FIGURE 5: (a–d) TEM images of $NiSb_2O_6$ nanoparticles obtained at 800°C.

$$V_{\text{Alarm}} = (10{,}000)60\left(\frac{1}{2} - \frac{516\,\Omega - \Delta R_S}{516\,\Omega + 516\,\Omega - \Delta R_S}\right) = V_{\text{Sat}}, \tag{8}$$

where V_{Alarm} and $V_{\text{Sat}} \approx 11.3\,V$ are the same value since the operational amplifier was in saturation due to the high gain A_{ol}. In this case, the signal alarm $V_{\text{Alarm}} \approx 11.3\,\text{V}$ was produced because the gas sensor detected the presence of the propane gas in the monitored atmosphere.

3. Results and Discussion

3.1. XRD Analysis. Figure 4 shows the diffractogram of the $NiSb_2O_6$ oxide calcined at 800°C. As it can be observed, the most intense reflections belong to the main phase of the oxide. The diffraction pattern obtained in this study was identified using the database's file JCPDF 38-1083 and PDF 86-0110. The material's characteristic planes were located at $2\theta = 19.22°$, $21.43°$, $27.14°$, $33.50°$, $34.99°$, $38.80°$, $40.19°$, $53.22°$, $56.03°$, $60.23°$, $62.77°$, $63.32°$, $67.20°$, $67.78°$, $73.89°$, $80.89°$, $83.13°$, and $86.83°$. According to the database's file, the $NiSb_2O_6$ oxide is a material that crystallizes in a tetragonal structure with network parameters $a = c = 4.641$ Å and $b = 9.219$ Å and space group P42/mnm (136). Additionally, reflections associated with NiO were found in the same diffractogram, located at $2\theta = 37.11°$, $43.25°$, and $75.27°$. These points were identified by means of the file JCPDF 01-1239. The NiO is a crystalline phase extraneous to the main reflections of the $NiSb_2O_6$, which crystallizes in a cubic structure with cell parameters $a = b = c = 4.1710$ Å and special group

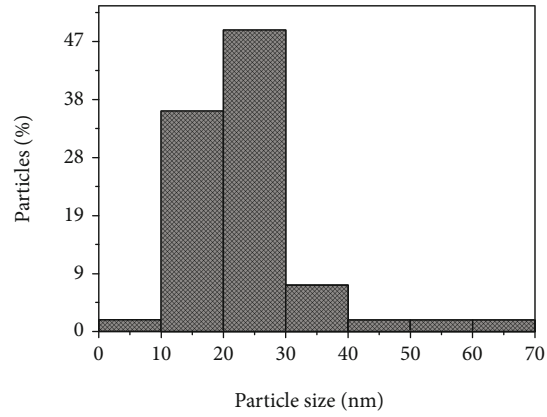

FIGURE 6: Size distribution of $NiSb_2O_6$ nanoparticles obtained at 800°C.

Fm-3m (JCPDF 01-1239). The results presented in Figure 4 are consistent with those reported in references [20, 24, 25], where the same compound was synthesized but following different preparation processes, like solid-state reaction or the colloidal route. In previous works, our research group reported the synthesis of $NiSb_2O_6$ applying wet chemistry processes [23–25, 27].

When we compare our XRD results with those reported in reference [27], where the crystalline phase of the same oxide was synthesized applying the solid-state reaction method at a temperature of 1450°C, it can be seen clearly that we obtained the crystalline phase of the $NiSb_2O_6$ at a significant lower temperature.

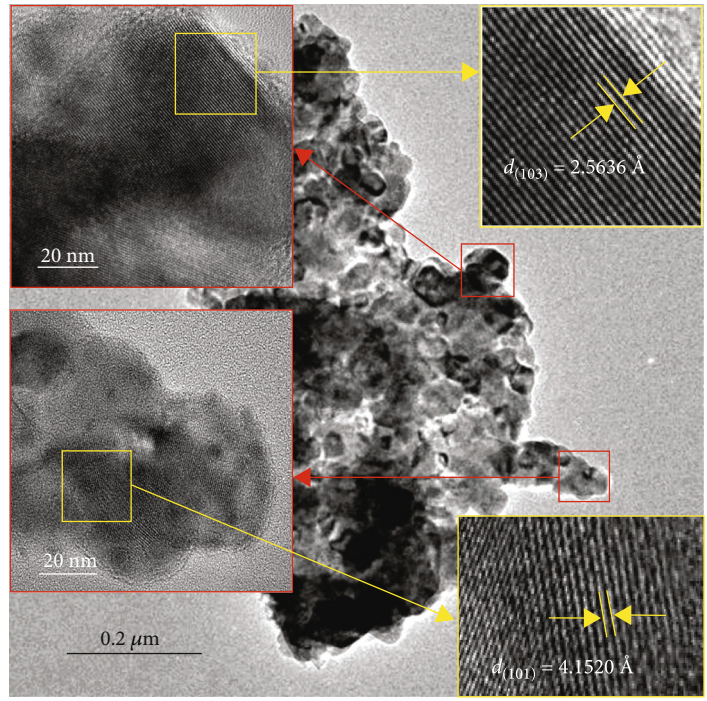

Figure 7: HRTEM images of the crystalline planes of the $NiSb_2O_6$ nanoparticles obtained at 800°C.

3.2. TEM Analysis. Figure 5 shows TEM images of the microstructure of the $NiSb_2O_6$ calcined at 800°C. The production of nanoparticles with different shapes and sizes is clearly discernible. The dark areas were due to the poor electron transmission on the particles. As can be observed in Figure 5(a), there is a large agglomeration of nanoparticles, which were joined by the effect of the temperature applied to the precursor material during the synthesis process. It can be seen that the nanoparticles are joined together due to the formation of necks caused by the coalescence of the particles, which is confirmed in Figure 5(b). The size of the nanoparticles was estimated in a range between 5 and 65 nm, with an average of ~23.24 nm and a standard deviation of ±10.7 nm (see Figure 6). The growth of very fine particles (average size of ~2.8 nm) on the nanoparticles can be observed. The growth of different morphologies can be discerned in Figures 5(c) and 5(d), as well as square-shaped particles embedded in the material, with an estimated size of ~78.57 nm.

Figure 7 shows high-resolution TEM (HRTEM) images of the surface of the $NiSb_2O_6$ nanoparticles calcined at 800°C. A zoom was made for identification of the particles' crystalline planes, estimating the size of the nanoparticles at 50.3 nm and at 21.62 nm for the neck-shaped particles. The formation of the planes indicated the crystalline nature of the material. In the case of the nanoparticles joined by necks, an orientation change of the crystalline planes can be observed. The distance d between the planes was estimated at 2.5636 and 4.1520 Å, corresponding, respectively, to the planes (103) and (101) of the tetragonal trirutile structure of the $NiSb_2O_6$. These planes had a maximum diffraction angle 2θ of 34.991 and 21.418°, which can be verified in Figure 4. These results corroborated the formation of the trirutile-type crystalline phase of the oxide.

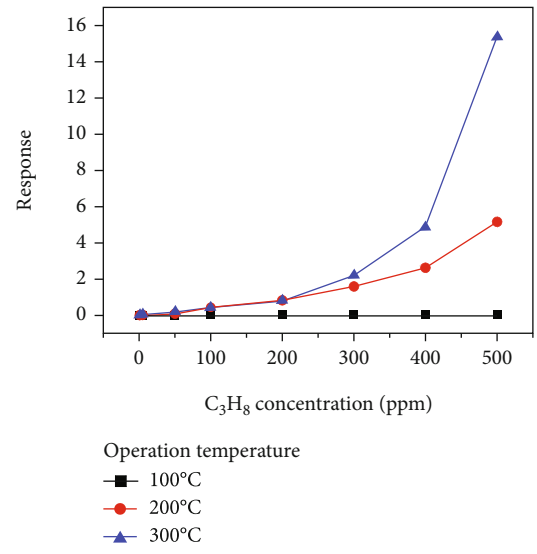

Figure 8: Response of the $NiSb_2O_6$ in the tests of sensitivity vs. C_3H_8 concentration.

3.3. Sensing Property Analysis. The analysis of the gas sensing properties of the nanostructured $NiSb_2O_6$ was done at 0, 1, 5, 50, 100, 200, 300, 400, and 500 ppm of propane and at temperatures of 100, 200, and 300°C. Sensitivity was calculated with equation (1) [23–25]. The results are depicted in Figure 8.

$NiSb_2O_6$ was clearly sensitive to each gas concentration and operating temperature. However, there were no significant variations at 100°C. However, as the temperature increased, the sensitivity's magnitude rose significantly. This is corroborated in Figure 8, where the magnitude at 200°C

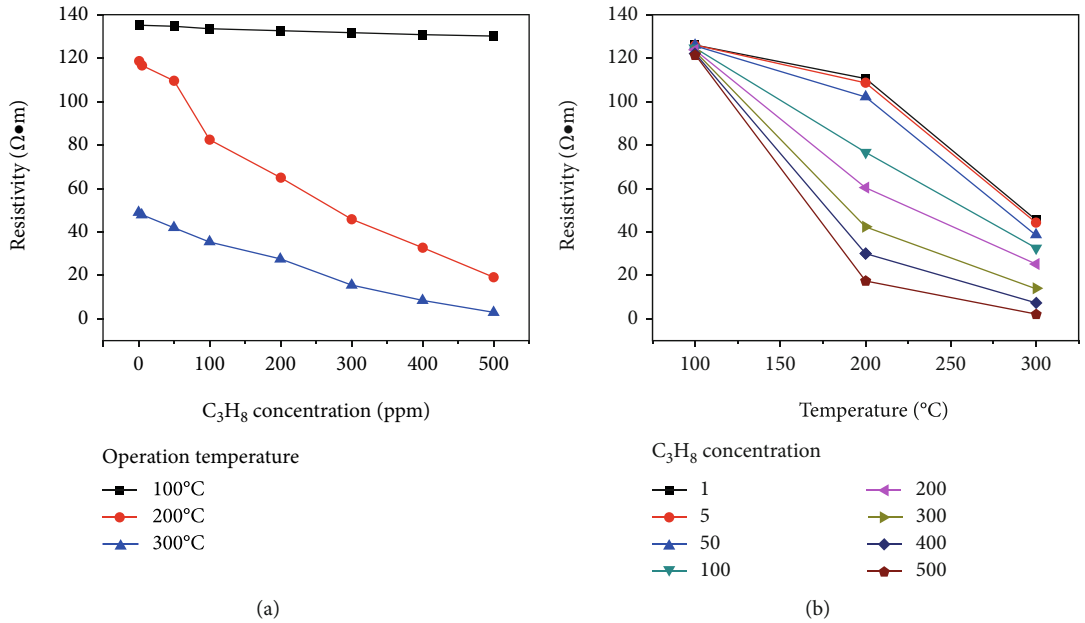

Figure 9: Electrical response (resistivity) of $NiSb_2O_6$ pellets as a function of (a) C_3H_8 concentration and (b) operating temperature.

was ~4.5. The maximum sensitivity value was ~15.5 at 300°C and 500 ppm of C_3H_8. The increase in material's sensitivity is caused by the rise in the number of gas molecules that react with the adsorbed oxygen, donating electrons to the material's surface [28]. In addition, the $NiSb_2O_6$'s response is associated with the oxygen desorption mechanism at high temperatures [29]. When the tests were performed at temperatures below 200°C, conditions were not enough to provoke oxygen desorption reactions (mainly O_2^- adsorption) [30]; therefore, an electric response did not occur regardless of gas concentration. However, by increasing the temperature to 300°C, the thermal energy was enough to form O^- and O^{2-} [31], which caused a greater interaction between the material's surface and the gas molecules, leading to an increase in material's sensitivity [32]. The high sensitivity of the $NiSb_2O_6$ is attributed to the nanometric particle size achieved during the synthesis process.

The electrical characterization, by testing resistivity (ρ) changes of $NiSb_2O_6$ pellets, was done in the presence of propane concentrations at different operating temperatures (100–300°C). To estimate the changes in the electrical resistivity ρ, the formula of reference [33] was used: $\rho = RA/t$, where R is the electrical resistance in the test gases, A is the area of the cross section, and t is the thickness of the pellets (0.5 mm thick, 12 mm in diameter).

Figure 9 shows the results of plotting resistivity vs. concentration and operating temperature. According to Figures 9(a) and 9(b), it can be verified that as the operating temperature increased, the electrical resistivity decreased and, therefore, the conductivity of the material increased. The resistivity changes of the $NiSb_2O_6$ are due mainly to the fact that with the increase in temperature, the pellets' surface shows oxidation due to the oxygen present during the test [31, 34], which provokes great mobility of the charge carriers and, therefore, an increase in the conductivity of the material [34, 35]. We

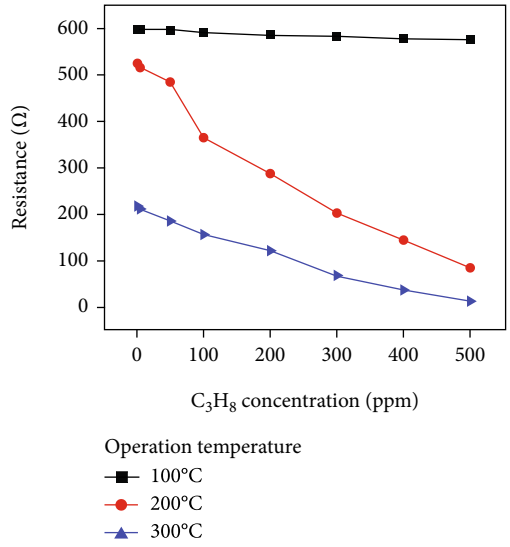

Figure 10: Plot of electrical resistance vs. C_3H_8 concentration (ppm) of the chemical sensor based on the $NiSb_2O_6$ oxide.

observed during the experiments that by increasing propane concentration (1 to 500 ppm) and temperature, greater diffusion of the test gas molecules occurred, favoring the decrease in electrical resistivity [23, 34]. This behavior is typical of a p-type semiconductor [20].

This behavior is attributed to the fact that the propane molecules increased their kinetic activity on the pellets' surface due to the operating temperature [34, 36, 37], which in our case was 200 and 300°C. Some authors have reported that changes in electrical response of a material like the one used in this work depend strongly on temperature, type of test gas, and sensor's geometric shape (like pellets and thick or thin films) [34, 35], all of which play a very important role in the gas detection mechanism. The results presented in Figure 9

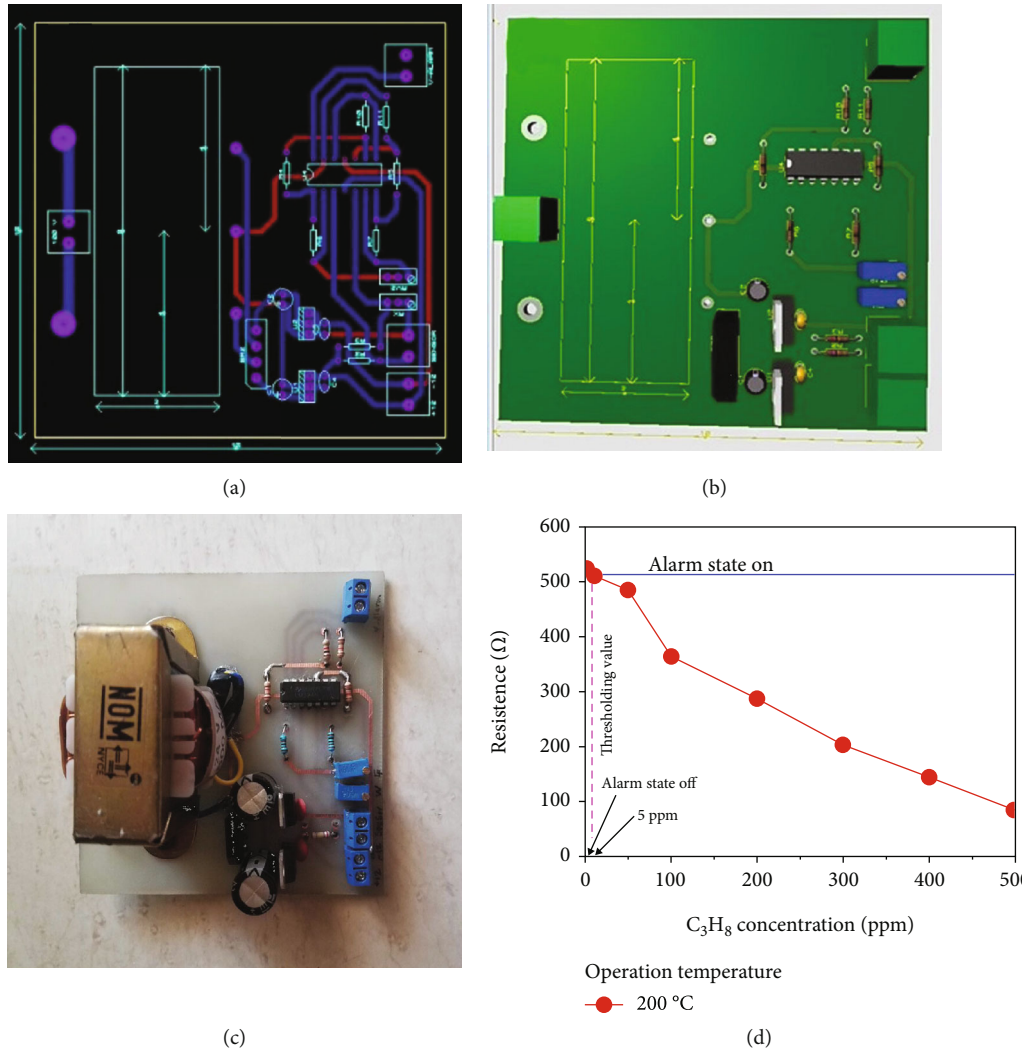

Figure 11: Economic target produced for our new detector device: (a) printed circuit board (PCB); (b) 3D proposal for the electronic components' distribution; (c) implemented target; (d) operation principle of our device.

are consistent with other studies reported in the literature for semiconductors similar to $NiSb_2O_6$ [23, 24, 30].

In particular, the electrical resistivity at 100°C was very high, with an almost linear behavior. It is clear that, at this temperature, the propane molecules could not react with the pellets' surface, provoking a poor material's response. In contrast, by increasing the operating temperature to 200°C, an increase in conductivity was recorded. Due to such temperature increase, the pellets showed an inflection point at 200°C, showing the most pronounced changes in electrical resistivity. When the temperature was raised to 300°C, the electrical conductivity increased considerably because the available thermal energy made the oxygen react during the test, causing a decrease in the electrical resistivity. At that point, the resistivity was 3.03 Ω·m at 500 ppm of propane. The high response of the $NiSb_2O_6$ pellets is attributed to the nanometric particle size obtained during the synthesis process.

When comparing the results of Figures 8 and 9 with other binary (like tin dioxide) and ternary (like our $NiSb_2O_6$) semiconductor oxides that have been proposed as gas sensors [20, 24, 36], we see that the $NiSb_2O_6$ oxide (which possesses a trirutile-type structure) showed greater response and thermal stability in propane atmospheres at concentrations of 1–500 ppm and at temperatures of 100, 200, and 300°C.

3.4. Resistance vs. C_3H_8 Concentration. From the resistivity response shown in Figure 9(a), the electrical resistance of our sensor was calculated applying the formula $R = \rho t/A$, where R is the electrical resistance in the test gases, ρ is the resistivity, t is the thickness of the pellets (0.5 mm thick, 12 mm in diameter), and A is the area of the cross section. The behavior of the resistance vs. C_3H_8 concentration was calculated and graphed in Figure 10.

Observing Figure 10, when the chemical sensor detects the propane gas, its electrical resistance decays for the three operating temperatures. The highest resistance was recorded at 100 and 200°C, whereas a lower resistance was recorded at 300°C. Therefore, our sensor had better sensitivity at 200 and 300°C (see Figure 8), with the resistance in the intervals 218–13.45 Ω and 525–85.32 Ω, respectively.

3.5. Operating Device. Figure 1 shows the electronic diagram of our propane detector, whose operating parameters were as follows: temperature of 200°C (see Figure 9(a)), gas concentration of 5 ppm (see Figure 11), circuit's gain of 5 (see Figure 1 and equation (3)), sensor's resistance of $R_S = 516\,\Omega$ (see Figures 10 and 11), and sensor's sensitivity of $S \approx 0.41$ (see Figure 8). Figure 11 depicts the electronic device and its operation. The printed circuit board (PCB), whose size was 10×10 cm, developed using the program Proteus®, is shown in Figure 11(a). Figure 11(b) shows the 3D proposal and the electronic component distribution, also developed using Proteus®. The implemented propane detection device can be observed in Figure 11(c), whose design is based on the 3D proposal. The device works as Figure 11(d) illustrates. Based on Figure 11(d), if the C_3H_8 concentration is equal or greater than 5 ppm, the sensor's resistance diminishes and the Wheatstone bridge is set unbalanced, causing the comparator circuit to generate the alarm signal $V_{\text{Alarm}} \approx V_{\text{Sat}}$. This generated voltage indicates "on alarm state." But if the C_3H_8 concentration is lower than 5 ppm, equation (2) is satisfied and the alarm signal is close to zero ($V_{Alarm} \approx 0$), indicating "alarm state off." It is worth mentioning that the sensitivity of our propane detector device can be improved through the R_{Gain}: if $R_{\text{Gain}} < 500\,\Omega$, the device will increase its sensitivity, but if $R_{\text{Gain}} > 500\Omega$, the sensitivity will be reduced. Finally, the gas detector could operate between 1 and 500 ppm by calibrating the Wheatstone bridge through the resistance R_{Cal}.

4. Discussion

In reference [23], a carbon monoxide (CO) detector based also on antimonite nickel was proposed, which could be applicable in atmospheric environments where the combustion in air of propane (liquid) already occurred. In the present work however, our goal was precisely the prevention of explosive catastrophes. Therefore, we proposed an economical and easy-to-implement propane gas detector, where the nickel antimonite could be applied as a gas sensor in an analog circuit based on the oxide's electrical response. So, comparing both proposals, our detector was focused on the prevention of catastrophes in order to avoid possible human and economic losses, while the detector of reference [23] was only focused on monitoring possible human intoxications by carbon monoxide due to explosions that already could take place. In such a manner, our future work has three directions: (1) application of the $NiSb_2O_6$ oxide in the quasidistributed detection of propane gas and carbon monoxide, (2) development of more efficient electronic devices for gas sensing based on nickel antimonite, and (3) reduction of the device's operating temperature.

5. Conclusions

In this work, a novel propane detection device was proposed, built, and tested. Our device possesses low cost, versatility, high sensitivity, good performance, fast response, selectivity, adaptability, propane (C_3H_8) concentration detection between 1 and 500 ppm, operating temperatures of 200 and 300°C (optimal temperature operation at 200°C), dimensions of 10 $\times$ 10 cm, AC supply voltage (120 volts), and output voltage called "alarm voltage" ($V_{\text{Alarm}} \approx 11.2$ volts). The prototype system consisted of an analog circuit which required a Wheatstone bridge, an instrumentation amplifier, a comparator, and a DC supply source, while the chemical sensor was based on the $NiSb_2O_6$ oxide: $NiSb_2O_6$ powders were synthetized through the colloidal method, characterized by XRD, its microstructure was observed using TEM, the particle size was measured from the TEM image, and its electrical response was proven through static electrical tests.

In summarized form, our propane gas detection system has some important features:

(1) The device can detect propane concentrations in extended intervals. The concentration value can be selected through the potentiometer R_{Cal}

(2) Sensitivity and response time can be increased using the potentiometer R_{Gain} (see Figure 1)

(3) The detector can operate efficiently at relatively low temperatures, being ideal for industrial applications

(4) Its supply voltage is 120 V (AC), and its output signal is ≈11.3 V (DC)

(5) The detector has low cost, easy implementation, excellent sensitivity, and fast response

All these characteristics make our proposed detection system an excellent candidate for being used in industry and other areas where the leakage of propane gas could be a risk.

Data Availability

The data related to the results that support our conclusions are available upon request to the authors. It can be done via e-mail. We will be pleased to respond.

Conflicts of Interest

The authors declare no conflict of interest.

Acknowledgments

The authors thank Mexico's National Council of Science and Technology (CONACyT) and University of Guadalajara for the support granted. Antonio Casillas Zamora and Jorge Alberto Ramírez Ortega also thank CONACyT for the scholarships. We thank M. de la Luz Olvera Amador for her technical assistance. This investigation was carried out following the line of research "Nanostructured Semiconductor Oxides" of the academic group UDG-CA-895 "Nano-structured Semiconductors" of CUCEI, University of Guadalajara.

References

[1] B. Bengherbie, M. O. Zmirli, A. Toubul, and A. Guessoum, "FPGA-based wireless sensor nodes for vibration monitoring system and fault diagnosis," *Measurement*, vol. 10, pp. 81–92, 2017.

[2] W. Wang, J. Xu, H. Zheng et al., "A spring-assisted hybrid triboelectric-electromagnetic nanogenerator for harvesting low-frequency vibration energy and creating a self-powered security system," *Nanoscale*, vol. 10, no. 30, pp. 14747–14754, 2018.

[3] M. Morisawa and S. Muto, "Plastic optical fibre sensing of fuel leakage in soil," *Journal of Sensors*, vol. 2012, Article ID 247851, 6 pages, 2012.

[4] C. Hou, J. Li, D. Huo et al., "A portable embedded toxic gas detection device based on a cross-responsive sensor array," *Sensors and Actuators B: Chemical*, vol. 161, no. 1, pp. 244–250, 2012.

[5] T. Schuller, T. Poinsot, and S. Candel, "Dynamics and control of premixed combustion systems based on flame transfer and describing functions," *Journal of Fuid Mechanics*, vol. 894, article P1, 2020.

[6] K. Wetchakun, T. Samerjai, N. Tamaekong et al., "Semiconducting metal oxides as sensors for environmentally hazardous gases," *Sensors and Actuators B*, vol. 160, no. 1, pp. 580–591, 2011.

[7] P. T. Moseley, "Materials selection for semiconductor gas sensors," *Sensors and Actuators B: Chemical*, vol. 6, no. 1–3, pp. 149–156, 1992.

[8] A. Guillén-Bonilla, V. M. Rodríguez-Betancourtt, M. Flores-Martínez et al., "Dynamic response of $CoSb_2O_6$ trirutile-type oxides in a CO_2 atmosphere at low-temperatures," *Sensors*, vol. 14, no. 9, pp. 15802–15814, 2014.

[9] G. Fine, L. Cavanagh, A. Afonja, and R. Binions, "Metal oxide semi-conductor gas sensors in environmental monitoring," *Sensors*, vol. 10, no. 6, pp. 5469–5502, 2010.

[10] M. A. Basyooni, S. E. Zaki, S. Ertugrul, M. Yilmaz, and Y. Ramazan Eker, "Fast response of CO_2 room temperature gas sensor based on mixed-valence phases in molybdenum and tungsten oxide nanostructured thin films," *Ceramics International*, vol. 46, no. 7, pp. 9839–9853, 2020.

[11] T. Lin, X. Lv, S. Li, and Q. Wang, "The Morphologies of the semiconductor oxides and their gas-sensing properties," *Sensors*, vol. 17, p. 2779, 2017.

[12] M. Singh, B. C. Yadav, A. Ranjan, M. Kaur, and S. K. Gupta, "Synthesis and characterization of perovskite barium titanate thin film and its application as LPG sensor," *Sensors and Actuators B: Chemical*, vol. 241, pp. 1170–1178, 2017.

[13] E. E. Ateia, M. M. Arman, and M. Morsy, "Synthesis, characterization of $NdCoO_3$ perovskite and its uses as humidity sensor," *Applied Physics A*, vol. 125, no. 12, 2017.

[14] Y. Yin, Y. Shen, P. Zhou et al., "Fabrication, characterization and n-propanol sensing properties of perovskite-type $ZnSnO_3$ nanospheres based gas sensor," *Applied Surface Science*, vol. 509, article 145335, 2020.

[15] D. Ziegler, A. Marchisio, G. Ercolino, S. Specchia, and J. M. Tulliani, "Ammonia selective sensors based on cobalt spinel prepared by combustion synthesis," *Solid State Ionics*, vol. 337, pp. 91–100, 2019.

[16] S. Zhang, W. Jiang, Y. Li et al., "Highly-sensitivity acetone sensors based on spinel-type oxide ($NiFe_2O_4$) through optimization of porous structure," *Sensors and Actuators B: Chemical*, vol. 291, pp. 266–274, 2019.

[17] J. Patil, D. Nadargi, I. S. Mulla, and S. S. Suryavanshi, "Spinel $MgFe_2O_4$ thick films: a colloidal approach for developing gas sensors," *Materials Letters*, vol. 213, pp. 27–30, 2018.

[18] D. T. Maimone, A. B. Christian, J. J. Neumeier, and E. Granado, "Lattice dynamics of ASb_2O_6 (A=Cu,Co) with trirutile structure," *Physical Review B*, vol. 97, article 104304, 2018.

[19] N. Matsubara, F. Damay, B. Vertruyen et al., "Mn_2TeO_6: a distorted inverse trirutile structure," *Inorganic Chemistry*, vol. 56, no. 16, pp. 9742–9753, 2017.

[20] A. Singh, A. Singh, S. Singh, and P. Tandon, "Nickel antimony oxide ($NiSb_2O_6$): a fascinating nanostructured material for gas sensing application," *Chemical Physics Letters*, vol. 646, pp. 41–46, 2016.

[21] F. Liu, B. Wang, Y. Xue et al., "High-temperature NO_2 gas sensor based on stabilized zirconia and $CoTa_2O_6$ sensing electrode," *Sensors and Actuators B: Chemical*, vol. 240, pp. 148–157, 2017.

[22] P. T. Moseley, D. E. Williams, J. O. W. Norris, and B. C. Tofield, "Electrical conductivity and gas sensitivity of some transition metal tantalates," *Sensors and Actuators*, vol. 14, no. 1, pp. 79–91, 1988.

[23] J. T. Guillen Bonilla, H. Guillen Bonilla, V. M. Rodríguez Betancourtt et al., "Carbone monoxide (CO) detection device based on the nickel antimonate oxide and a DC electronic circuit," *Applied Sciences*, vol. 9, p. 17, 2019.

[24] V. M. Rodríguez Betancourtt, H. Guillen Bonilla, M. Flores Martínez et al., "Gas sensing properties of $NiSb_2O_6$ micro- and nanoparticles in propane and carbon monoxide atmospheres," *Journal of Nanomaterials*, vol. 2017, Article ID 8792567, 9 pages, 2017.

[25] H. Guillen Bonilla, M. de la Luz Olvera Amador, Y. L. C. Moreno et al., "Synthesis and characterization of nickel antimonate nanoparticles: sensing properties in propane and carbón monoxide," *Journal of Materials Science: Materials in Electronics*, vol. 30, pp. 6166–6177, 2019.

[26] L. Gildo-Ortiz, H. Guillén-Bonilla, J. Santoyo-Salazar et al., "Low-temperature synthesis and gas sensitivity of perovskite-type $LaCoO_3$ nanoparticles," *Journal of Nanomaterials*, vol. 2014, Article ID 164380, 8 pages, 2014.

[27] H. Ehrenberg, G. Wltschek, J. Rodriguez-Carvajal, and T. Vogt, "Magnetic structures of the tri-rutiles $NiTa_2O_6$ and $NiSb_2O_6$," *Journal of Magnetism and Magnetic Materials*, vol. 184, no. 1, pp. 111–115, 1998.

[28] L. Gildo-Ortiz, H. Guillén-Bonilla, V. M. Rodríguez-Betancourtt et al., "Key processing of porous and fibrous LaC_oO_3 nanostructures for successful CO and propane sensing," *Ceramics International*, vol. 44, no. 13, pp. 15402–15410, 2018.

[29] H. J. Kim and J. H. Lee, "Highly sensitive and selective gas sensors using p-type oxide semiconductors: overview," *Sensors and Actuators B: Chemical*, vol. 192, pp. 607–627, 2014.

[30] H. Guillén-Bonilla, M. Flores-Martínez, V. M. Rodríguez-Betancourtt et al., "A novel gas sensor based on $MgSb_2O_6$ nanorods to indicate variations in carbon monoxide and propane concentrations," *Sensors*, vol. 16, no. 2, p. 177, 2016.

[31] S. C. Chang, "Oxygen chemisorption on tin oxide: correlation between electrical conductivity and EPR measurements," *Journal of Vacuum Science and Technology*, vol. 17, pp. 366–369, 1979.

[32] G. Carbajal-Franco, A. Tiburcio-Silver, J. M. Domínguez, and A. Sánchez-Juárez, "Thin film tin oxide-based propane gas sensors," *Thin Solid Films*, vol. 373, no. 1-2, pp. 141–144, 2000.

[33] J. Kita, A. Engelbrecht, F. Schubert, A. Grob, F. Rettig, and R. Moos, "Some practical points to consider with respect to

thermal conductivity and electrical resistivity of ceramic substrates for high-temperature gas sensors," *Sensors and Actuators B: Chemical*, vol. 213, pp. 541–546, 2015.

[34] A. Guillén-Bonilla, V. M. Rodríguez-Betancourtt, J. T. Guillén-Bonilla et al., "A novel CO and C_3H_8 sensor made of $CuSb_2O_6$ nanoparticles," *Ceramics International*, vol. 43, no. 16, pp. 13635–13644, 2017.

[35] J. F. McAleer, P. T. Moseley, J. O. W. Norris, and D. E. Williams, "Tin dioxide gas sensors. Part 1.—aspects of the surface chemistry revealed by electrical conductance variations," *Journal of the Chemical Society, Faraday Transactions 1: Physical Chemistry in Condensed Phases*, vol. 83, no. 4, pp. 1323–1346, 1987.

[36] H. Gómez-Pozos, J. L. González-Vidal, G. Alberto-Torres, M. De la Luz Olvera, and L. Castañeda, "Physical characterization and effect of effective surface area on the sensing properties of tin dioxide thin solid films in a propane atmosphere," *Sensors*, vol. 14, pp. 403–415, 2014.

[37] C. Wang, L. Yin, L. Zhang, D. Xiang, and R. Gao, "Metal oxide gas sensors: sensitivity and influencing factors," *Sensors*, vol. 10, no. 3, pp. 2088–2106, 2010.